NeuroImage 244 (2021) 118563

Contents lists available at ScienceDirect

NeuroImage

journal homepage: www.elsevier.com/locate/neuroimage

Functional coupling between CA3 and laterobasal amygdala supports schema dependent memory formation

Mushfa Yousuf[a], Pau A. Packard[b], Lluís Fuentemilla[c,d,e], Nico Bunzeck[a,f,*]

[a] Department of Psychology, University of Lübeck, Lübeck 23562, Germany
[b] Center for Brain and Cognition, Department of Information and Communication Technologies, Universitat Pompeu Fabra, Roc Boronat, Barcelona 08005, Spain
[c] Cognition and Brain Plasticity Group, Bellvitge Biomedical Research Institute (IDIBELL), Hospitalet de Llobregat, Spain
[d] Department of Cognition, Development and Educational Psychology, University of Barcelona, Barcelona, Spain
[e] Institute of Neurosciences, University of Barcelona, Barcelona, Spain
[f] Center of Brain, Behavior and Metabolism (CBBM), University of Lübeck, Ratzeburger Allee 160, Lübeck 23562, Germany

ARTICLE INFO

Keywords:
Congruence effect
Schema
Medial temporal lobe
Subfields
Amygdala

ABSTRACT

The medial temporal lobe drives semantic congruence dependent memory formation. However, the exact roles of hippocampal subfields and surrounding brain regions remain unclear. Here, we used an established paradigm and high-resolution functional magnetic resonance imaging of the medial temporal lobe together with cytoarchitectonic probability estimates in healthy humans. Behaviorally, robust congruence effects emerged in young and older adults, indicating that schema dependent learning is unimpaired during healthy aging. Within the medial temporal lobe, semantic congruence was associated with hemodynamic activity in the subiculum, CA1, CA3 and dentate gyrus, as well as the entorhinal cortex and laterobasal amygdala. Importantly, a subsequent memory analysis showed increased activity for later remembered vs. later forgotten congruent items specifically within CA3, and this subfield showed enhanced functional connectivity to the laterobasal amygdala. As such, our findings extend current models on schema dependent learning by pinpointing the functional properties of subregions within the medial temporal lobe.

1. Introduction

The processing of congruent semantic information promotes long-term memory (Bartlett, 1932; Bower, 1972). This so-called 'congruence effect' can be explained by the integration of information into knowledge structures or schemas (see also Piaget, 1952). More recent work further suggests that, during the encoding of information, a congruent semantic match may be an initial step in a general schema-dependent process of memory integration (Gilboa and Marlatte, 2017; Robin and Moscovitch, 2017; Spalding et al., 2015; van Kesteren et al., 2012). Importantly, on the neural level, this is supposed to entail functional processes within the medial temporal lobe (MTL) possibly in concert with other brain regions, such as the prefrontal cortex (PFC), leading to more efficient consolidation of congruent events (Gilboa and Marlatte, 2017). However, the precise contribution of the MTL, including hippocampal subfields (see below) and surrounding cortex, still remains unclear.

A series of animal studies showed that the hippocampus plays a critical role in the integration of novel information into existing representations (Tse et al., 2011, 2007). Specifically, rats learned flavor-place associations over several weeks and therefore gradually established a neocortical and hippocampus-independent representation of these paired-associations. Subsequently, new paired associations within the same spatial layout could be learned in a single trial session and recalled even after 24 h suggesting a rapid integration of novel information into pre-existing schemas. Importantly, the recall of new paired associations was hippocampus independent already after 24 h suggesting a rapid transfer of information from the MTL to the neocortex.

Further evidence for a role of the MTL in schema dependent learning (or semantic congruence encoding) comes from human studies using functional magnetic resonance imaging (fMRI). They not only show enhanced long-term memory of schema-congruent information but also a modulation in connectivity between the hippocampus and other cortical regions, most prominently the medial PFC (Kesteren et al., 2010; Sommer, 2017; M.T.R. van Kesteren et al., 2013). According to the Schema-Linked Interactions between Medial prefrontal and Medial temporal regions (SLIMM) model (van Kesteren et al., 2012), the mPFC "resonates" with congruent information and therefore inhibits MTL activity in order to drive semantic integration. Although there is some evidence in favor of activation patterns compatible with SLIMM (van Kesteren et al., 2014; M.T.R. 2013, 2012), other work suggests the MTL plays

* Corresponding author.
E-mail address: nico.bunzeck@uni-luebeck.de (N. Bunzeck).

https://doi.org/10.1016/j.neuroimage.2021.118563.
Received 16 June 2021; Received in revised form 6 September 2021; Accepted 6 September 2021
Available online 17 September 2021.

a more active role in the integration of semantic congruent information (Gilboa and Marlatte, 2017; Liu et al., 2017; McKenzie et al., 2014; S. 2013; Preston and Eichenbaum, 2013; van Kesteren et al., 2020).

The MTL can be subdivided into the hippocampus and surrounding cortex, including entorhinal (EC), perirhinal (PC) and parahippocampal (PHC) cortex (Andersen et al., 2006; Squire et al., 2004; Witter et al., 1989). Within the hippocampus, the most prominent signaling pathway is a trisynaptic circuit and includes a projection from EC to the dentate gyrus (DG) via the perforant path, from DG to CA3 via mossy fibers, and from CA3 to CA1 via Schaffer collaterals (Amaral, 1993; Lavenex and Amaral, 2000). At the functional level, DG delineates similar incoming information, called pattern separation, in order to be encoded, stored and retrieved in CA3 (Jonas and Lisman, 2014; Senzai, 2019). Specifically, in computational models, CA3 functions as “single attractor” or “autoassociation network”, which allows rapid encoding (and storage) of episodic information through associations, which can subsequently be retrieved through pattern completion (Grande et al., 2019; Rolls, 2013a, 2013b). CA1, on the other hand, is supposed to compare incoming sensory information with predictions provided by CA3 and therefore serves as a “comparator” (Lisman and Grace, 2005). In the case of a mismatch, a neural novelty signal drives hippocampal encoding (Hasselmo and Wyble, 1997; Chen et al., 2011).

Finally, the amygdala, which can be subdivided into different nuclei, is located adjacent to the anterior part of the MTL with prominent connections from parahippocampal, entorhinal, and hippocampal cortices (Pitkänen et al., 2000; Ruiz-Rizzo et al., 2020; Strange et al., 2014). Functionally, the amygdala was typically linked to emotional processing and fear learning (LeDoux, 2014), but also novelty processing (Rutishauser et al., 2006; Sheth et al., 2008) and subsequent memory formation for emotionally neutral items (Rutishauser et al., 2010). However, the role of specific nuclei in congruence dependent learning is little understood. Taken together, MTL subregions are highly interconnected, functionally specialized and yet, serve complementary functions. Therefore, semantic congruence processing and related memory enhancement may be based on specific MTL subregions and the interconnected amygdala.

Functional properties of MTL subregions in schema dependent learning is scarce and mainly comes from animal studies. For instance, in rats neural firing patterns indicative of a full schema representation were evident in both hippocampal subfields CA1 and CA3 (McKenzie et al., 2014). A distinction between both regions could also be observed on the level of specific features including item information and position (McKenzie et al., 2014). Together with work from the same group, also in rats (Komorowski et al., 2013, 2009; S. McKenzie et al., 2013), this suggests that both CA1 and CA3 underlie congruency processing and schema dependent memory enhancement.

While most previous studies on schema-dependent learning have focused on younger participants (i.e., 18–35 years), potential age-related changes and associated neural mechanisms remain unclear. While age-related impairments could be expected on the basis of well-described memory deficits in older adults, it is also clear that semantic memory (i.e., long-term memory for facts independent of time and date) is often preserved until old age (Hedden and Gabrieli, 2004). In a recent study using electroencephalography (EEG), we showed that semantic congruence increases long-term memory in a group of healthy young and older adults, and, at the neural level, this could be linked to neural oscillations in the theta, alpha and beta range (4–20 Hz), as well as ERPs that were previously associated with semantic processing (Packard et al., 2020). Others have shown that the effect of congruence on long-term memory can be impaired during healthy aging (Amer et al., 2019, 2018), which was associated with overactivation in older adults as measured with fMRI (Amer et al., 2019). Since the MTL typically degenerates with age, starting at around 50 years (Raz et al., 2004), we also aimed to investigate the effect of age on semantic congruence processing and related memory formation.

Here, we used a previously established paradigm (Packard et al., 2020, 2017) in combination with high-resolution fMRI of the MTL to investigate the role of MTL subregions in schema dependent learning. In the encoding phase, which took place in the MRI scanner, subjects were presented with a series of semantic category words (e.g., furniture) that were individually followed by another word that could be semantically congruent (e.g., desk) or incongruent (e.g., guitar). In a recognition memory phase, ca. 20 min after leaving the MRI scanner, semantically congruent and incongruent words were randomly presented with a set of previously unstudied distractors and subjects indicated whether the word was old or new (see methods). We hypothesized (a) that semantic congruence drives long-term memory across the life span, (b) increased MTL activation for semantic congruence, and (c) a subsequent memory effect (i.e., increased activation for later recognized semantically congruent items) within CA3 and possibly CA1. We also predicted and explored enhanced connectivity between MTL subregions showing the subsequent memory effect.

2. Material and methods

2.1. Participants

Seventy-one healthy human subjects participated in our study. Data from nine subjects were discarded because they either did not understand the task ($n = 3$), did not wish to complete the measurement ($n = 6$), or because of technical issues during data acquisition ($n = 3$). Data from 33 young participants (age range 18–35 years, M = 24.42, SD = 3.75; female = 17) and 29 older participants (age range 50–80 years, M = 62.82, SD = 8.47; female = 15) were analyzed.

All older participants were assessed with the Montreal Cognitive Assessment (MoCA) version 7 (Nasreddine et al., 2005). Twenty-seven older participants scored 23 or higher (M = 26.59, SD = 1.75), whereas two older participants scored 21 on the MoCA test. Typically, a value of 22 should be considered as cut-off since this appears to be an appropriate cut-off for mild cognitive impairment (Freitas et al., 2013). However, since the two older participants who scored 21 did not show any unusual task performance (no outlying values for any measure), or any apparent brain degenerations, and in order to include as many participants as possible, they were kept in the analysis.

All participants were right-handed, had a normal or corrected-to-normal vision (including color vision), no history of neurological or psychiatric disorders (self-report), and were not taking any medication at the time. Participants were recruited through announcements in the local newspaper or the database of the University of Lübeck (Greiner, 2015). All participants signed a written informed consent and received monetary compensation. The study was approved by the local ethics committee of the University of Lübeck, Germany, and in accordance with the Declaration of Helsinki.

2.2. Stimuli and procedure

Following our previous work (Packard et al., 2020, 2017), participants performed a modified version of the Deese-Roediger-McDermott paradigm (Kim and Cabeza, 2007; Roediger and McDermott, 1995), which was programmed and presented using Presentation software (Neurobehavioral System Inc. Albany, CA). The experimental paradigm (Fig. 1) consisted of two stages: the encoding phase (inside the MRI scanner) and the recognition phase (outside the MRI scanner using a laptop, ca. 20 min after encoding).

Experimental stimuli consisted of 66 word lists from our previous study (Packard et al., 2020). Each list consisted of the 6 most typical instances (e.g., cow, pig, horse, chicken, sheep, and goat) of a natural/artificial category (e.g., farm animal). All of the 396 typical instances, semantically related to their respective semantic categories, were presented in separate encoding trials, each time preceded by a cat-

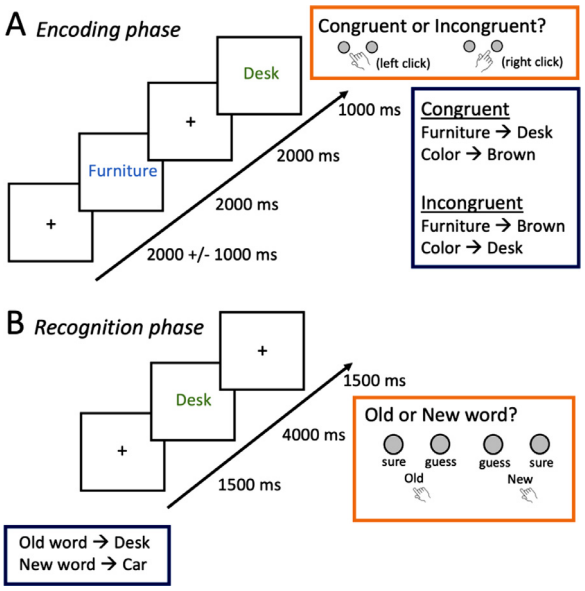

Fig. 1. Task overview. (A) Three hundred ninety-six trials were presented in the encoding phase. Each trial began with the presentation of a fixation cross, followed by a semantic category name in blue font, another fixation cross, and a word in green font. Participants were instructed to press a button indicating whether the second word was congruent (left click) or incongruent (right click) with the semantic category presented at the beginning of the trial. (B) Seven hundred ninety-two trials were presented in the recognition phase. Each trial began with a fixation cross followed by a word in green font. After each word, participants responded by pressing one of 4 keys according to whether the word was judged to be "sure old," "guess old," "guess new," or "sure new.".

egory (semantic cue). Additionally, semantically unrelated words were used as control words (new words) in the test phase.

The study phase consisted of 396 separate word-encoding trials, presented mixed in random order. Each trial started with the appearance of a fixation cross on the screen for a random duration of 2000–3000 ms. Subsequently, a category name in blue appeared on a white background for 1500 ms. After the cue disappeared, a fixation cross appeared for 2000 ms. Participants were then sequentially shown the subsequent word in green for 1000 ms. In the congruent condition, the subsequent word belonged to the semantic category (Craik and Tulving, 1975), for example, 'furniture' followed by 'desk'. In the incongruent condition, the category name did not correspond to the subsequent word, for example 'planets' followed by 'cottage'. While the second word was shown, the participants pressed a button indicating whether the word was congruent (left click) or incongruent (right click) with the semantic category presented at the beginning of the trial. Participants were instructed to respond as quickly and correctly as possible.

There were 198 congruent-list trials and 198 incongruent-list trials. Together, the study phase lasted about 60 min. At the end of this phase and outside the MRI scanner, participants were presented with a distraction task in which they solved simple arithmetical problems (additions and subtractions) in order to avoid an active rehearsal of the previously presented words. The distraction task lasted approximately 5 min, which, together with the explanations for it and for the subsequent recognition test as well as the anatomical scans at the end of the encoding phase (see below) made for a total time interval of 20 min between encoding and the subsequent test.

In the memory recognition test, participants were tested using 396 old words (i.e., all words from the encoding phase) and 396 new words presented in random order. Each of the 792 trials started with a fixation cross in the screen center (1500 ms) followed by a word. All words were displayed in the middle of the screen, in green and same font and size as the study phase, each for 4000 ms. After each word, participants responded by pressing one of 4 keys according to whether the word was judged to be "sure old," "guess old," "guess new," or "sure new." The scale graduations were color-coded on the keyboard and participants were instructed to respond within 4000 ms. Every 50 trials the participants could take a short break. The test phase had a duration of 60 min approximately.

2.3. MR data acquisition

Structural and functional imaging was performed on a 3-T Siemens MAGNETOM Skyra whole-body scanner (Siemens Healthcare, Erlangen, Germany) using a 32-channel head coil at the center for brain behavior and metabolism (CBBM), Universität zu Lübeck. Functional images were acquired in a simultaneous multi-slice fashion with a gradient-echo EPI sequence (voxel dimensions 1.5 × 1.5 × 1.5 mm, 28 slices, 864 × 864 matrix size, TE = 26 ms, TR = 1.1 s, 60° flip angle, 1.5 mm slice thickness). Five additional dummy volumes, which were subsequently discarded, were acquired at the beginning of each experimental block to account for equilibrium effects. Given our a priori hypothesis (see introduction), we acquired only a partial volume of the brain including the medial temporal lobe, covering hippocampus, surrounding cortex and amygdala. Note besides, the voxel size should be proportional to the signal to noise ratio (SNR) of fMRI blood oxygenation level-dependent signals, and smaller voxel size could be adapted with either longer scan time (i.e., TR) or higher SNR (Murphy et al., 2007; Edelstein et al., 1986). Here, in the current study, a partial volume would not only give us the advantage of maintaining the balance between smaller TR and higher spatial resolution but it also might increase the SNR within the regions of interest (Amaro and Barker, 2006).

To improve EPI data quality, field map imaging was performed before the start of the first and fourth experimental block with a double-echo spoiled gradient-echo sequence (gre_field_map; 104 × 104 matrix size TR = 0.61 s, TE_1 = 4.92 ms, TE_2 = 7.38 ms, voxel dimensions = 2 × 2 × 2 mm, 60° flip angle, 2 mm slice thickness), which generated a magnitude image and two-phase images. The field map image, which was used during preprocessing (see below), was computed from the two-phase images. Finally, whole-brain high-resolution structural images were acquired at the end of the MRI session, using a T1-weighted (voxel dimensions 1 × 1 × 1 mm, 256 × 256 matrix size, TE = 2.44 ms, TR = 1.9 s, 9° flip angle, 1 mm slice thickness) and T2-weighted pulse sequence (voxel dimensions 0.39 × 0.39 × 2 mm, 512 × 512 matrix size, TE = 92 ms, TR = 6.27 s, 150° flip angle, 2 mm slice thickness).

2.4. Behavioral data analysis

Behavioral data were analyzed using the jamovi software for macOS: the jamovi project (2020); jamovi (Version 1.2) (https://www.jamovi.org). For the encoding phase, we assessed response times, with a two-way mixed-design ANOVA with the factors age (young, old) and congruence (congruent, incongruent).

For the memory phase, we assessed recognition memory performance based on corrected high confidence hit rates, which were calculated by subtracting high confidence false alarms (i.e., erroneous sure responses to new words) from highly confident responses (i.e., sure old). Note that erroneous 'old' responses to words that were not actually presented during encoding could not be subdivided further into congruent vs. incongruent words; therefore, the same false-alarm rate was subtracted from hits for congruent and incongruent words. Given that memory impairments in older age might be particularly pronounced for high-confidence responses (Chua et al., 2009; Dodson et al., 2007; Shing et al., 2009), we specifically focused on high-confidence responses. Statistics (on corrected high-confidence hit rates) were performed using a two-way mixed-design ANOVA with factors age (young, old) and congruence (congruent, incongruent).

2.5. fMRI data analysis

Data preprocessing and analyses were performed using SPM12 (http://www.fil.ion.ucl.ac.uk/spm/software/spm12/) running on MATLAB R2018b (Mathworks, Natick, US). Slice timing correction for each block was carried out with reference to the middle slice using Fourier phase interpolation. Subsequently, voxel displacement maps (VDMs) were calculated using field maps for each subject individually. For the functional blocks 1 to 3, the VDM was computed using the field maps that were acquired before the start of the first experimental block; conversely, for the functional blocks 4 to 6, the VDM was calculated using the field maps that were acquired before the beginning of the fourth experimental block. The VDMs were then processed with "realignment & unwarp" to correct the distortions that occurred due to field inhomogeneities. Furthermore, volumes from all six functional blocks were spatially realigned to the first functional volume of the first block using rigid body transformation. In the next step, the mean functional image of the six blocks was co-registered to the structural T1 image of each subject. Finally, the normalization was performed using a diffeomorphic anatomical registration through exponentiated lie algebra (DARTEL) template (Ashburner, 2007). Segmentation of the T1 images was performed to produce DARTEL-compatible gray and white matter images for the tissue probability maps. A DARTEL template was then generated using the estimated gray and white matter of all participants. Finally, functional data were normalized to MNI space using the parameters produced by the DARTEL template with a smoothing factor of 3-mm FWHM. While different methods exist to normalize individual brains, using DARTEL appears to be advantageous especially in aging populations (Callaert et al., 2014) since it creates a group template on the basis of all (in this case young and older) subjects.

In a first model, we assessed the neural effects associated with congruence processing. Here, on the first level, for each participant an event-related design matrix was created containing the conditions of interest: semantic category words, congruent and incongruent words as well as errors. Each condition was separately modeled in the design matrix, and first-level contrast images were generated using a one-sample *t*-test for congruent and incongruent conditions separately. Furthermore, movement parameters estimated from realignment were also included as effects of no interest. Low-frequency noise was removed using a high-pass filter (cut-off 128 s). The standard SPM autoregressive AR(1) model was applied, and the onset regressors were convolved with the canonical hemodynamic response function. First-level contrast images were generated using a one-sample *t*-test for the congruent and incongruent condition. On the second (group) level, we conducted a two-way mixed-design ANOVA with the factors age (young, old) and congruence (congruent, incongruent). These analyses were specified as flexible factorial design in SPM12, with each participant treated as a random effect variable. Main effects were tested using t-contrasts, and two-way interaction using F-contrast.

In a second model, we assessed the neural effects associated with subsequent memory (i.e. behavior), also known as "Difference due to Memory" (or DM effect) (Paller et al., 1987). Here, we compared those words that could later be recognized (high confidence hits) vs. those that were subsequently forgotten for both conditions congruent and incongruent. Therefore, for each participant an event-related design matrix was created on the first level containing the conditions of interest: congruent later remembered vs. later forgotten (i.e., DM congruent sure) and incongruent later remembered vs. later forgotten (i.e., DM incongruent sure) words. Similar to our first model, we also included semantic category words, errors, and movement parameters. Additionally, we included subsequently recognized words with low confidence (i.e., correct 'old unsure' responses to congruent and incongruent stimuli) and subsequently not recognized words (i.e., incorrect 'new' responses). The congruent unsure and incongruent unsure regressors were entered into the general linear model (GLM) separately. Low-frequency noise was removed using a high-pass filter (cut-off 128 s), the standard SPM autoregressive AR(1) model was applied, and onset regressors were convolved with the canonical hemodynamic response function. First-level contrast images were generated using a one-sample *t*-test for DM congruent sure and DM incongruent sure. On the second (group) level, we carried out a two-way mixed-design ANOVA with the factors age (young, old) and congruence (DM congruent sure, DM incongruent sure). Main effects were tested using t-contrasts, and two-way interaction using F-contrast.

Furthermore, to specify the anatomical locations of our findings, SPM Anatomy toolbox version 2.2c (https://www.fz-juelich.de/inm/inm-1/DE/Forschung/_docs/SPMAnatomyToolbox/SPMAnatomyToolbox_node.html; (Eickhoff et al., 2007, 2006, 2005)) was used along with probabilistic cytoarchitectonic maps of the amygdala and MTL (Amunts et al., 2005). It allowed us to estimate the correlation between functionally activated clusters and architectonically defined probabilistic areas. Specifically, a functional cluster is first projected onto the probabilistic cytoarchitectonic maps, and subsequently the overlapping voxels are calculated as percentages. These percentages express the proportion of voxels assigned to each probabilistic cytoarchitectonic map relative to the total number of voxels in the activated functional cluster.

Finally, to better understand the hippocampal activation associated with the DM results (see results section), seed-based functional connectivity analysis was performed using the Beta Series Correlation toolbox (Göttlich et al., 2015). The functional cluster (i.e., seed region) was delineated using the MarsBar region-of-interest toolbox (Brett et al., 2002). BASCO toolbox is based on the approach introduced by Rissman et al. (2004). It uses a GLM with a separate covariate to model the evoked activity in each trial of the experimental condition resulting in beta-value series for each voxel. These beta-series are then used to estimate functional connectivity between brain regions of interest (Göttlich et al., 2015). In the current analysis, a GLM was first created and subsequently estimated for each participant individually. The regressors for congruent remembered high-confidence, congruent forgotten, incongruent remembered high-confidence, and incongruent forgotten trials were modeled in the GLM as conditions of interest. Additionally, congruent low-confidence remembered, incongruent low-confidence remembered, category words, errors, and movement parameters were included in the GLM as regressors of no interest. Following model estimation, the functional connectivity maps were estimated by correlating a mean beta-series from a seed region of interest to each voxel's beta series within the entire partial volume (i.e., the volume scanned) of the brain. The functional connectivity maps were estimated for each condition of interest (i.e., congruent high-confidence remembered, congruent forgotten, incongruent high-confidence remembered, and incongruent forgotten) separately on a single-subject level, and the resulting connectivity maps were Fisher z-transformed. Subsequently, DM congruent sure and DM incongruent sure contrasts were estimated, and then statistically analyzed at the group level (i.e., second level analysis). Similar to our DM analysis, a two-way mixed-design ANOVA was computed with the factors age (young, old) and congruence (DM congruent sure, DM incongruent sure). Here, we limited our focus on the overall main effect 'DM congruent sure vs. DM incongruent sure' since this contrast revealed functional activity within the hippocampus in the initial DM analysis. The average beta- and z-values of significant clusters were extracted for plotting using the MarsBar toolbox (Brett et al., 2002).

An explicit gray matter mask was used on the group-level analyses. The gray matter mask was created by first taking the mean of all spatially normalized gray matter images of all subjects (i.e., wc1*), and then the resultant mean image was thresholded using ImCal expression "i1>0.2″. This thresholded mean mask was defined as an explicit mask in all group-level analyses. Furthermore, an uncorrected voxel-level threshold of $p < .001$ was selected for all the analyses, with a family-wise error rate (FWE) corrected threshold of $p < .05$ at the cluster level.

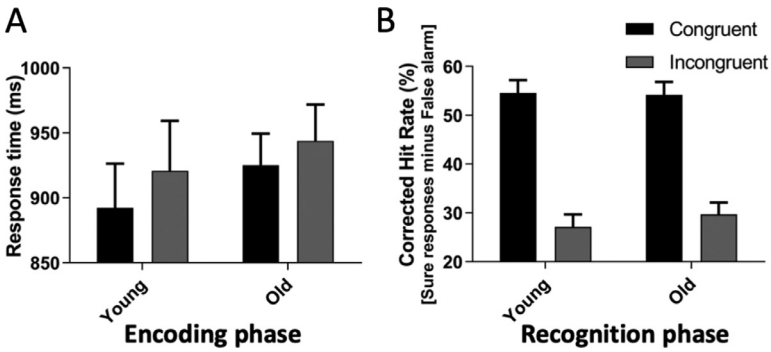

Fig. 2. Behavioral performance in the encoding and test phase of the task. Crossbars represent the mean (central line) plus-minus the standard error of the mean. (A) Response time in the encoding phase. (B) Percentage of correct responses in the test phase. We observed main effects of congruence on RTs and corrected hit rate but no main effects of age and no significant interactions between age and congruence, see text.

Table 1
Mean absolute numbers of correct responses and percentages at the test phase. Numbers in brackets represent one SEM.

Age	Old words			
		Sure	Unsure	Forgotten
Young	**Congruent**	128.81 (4.33)	33.81 (3.70)	31.69 (2.86)
		65.06 (2.18)%	17.08 (1.87)%	16.01 (1.44)%
	Incongruent	74.42 (4.65)	46.24 (4.47)	74.87 (4.06)
		37.58 (2.35)%	23.35 (2.25)%	37.81 (2.05)%
Old	**Congruent**	120.93 (5.04)	25.58 (4.24)	46.86 (3.72)
		61.07 (2.54)%	12.92 (2.14)%	23.66 (1.88)%
	Incongruent	72.44 (5.27)	28.58 (4.50)	93.51 (4.73)
		36.59 (2.66)%	14.43 (2.27)%	47.23 (2.38)%
	New words		**False alarm**	
Young	**Sure**	**Unsure**	**Sure**	**Unsure**
	236.60 (16.54)	117.33 (13.39)	12.15 (2.71)	29.27 (3.72)
	59.74 (4.17)%	29.63 (3.38)%	3.06 (0.68)%	7.39 (0.93)%
Old	325.37 (12.92)	41.51 (10.10)	12.51 (2.13)	14.79 (3.48)
	82.16 (3.26)%	10.48 (2.55)%	3.16 (0.53)%	3.73 (0.88)%

3. Results

3.1. Behavioral results

A two-way mixed-design ANOVA with the factors age (young, old) and congruence (congruent, incongruent) on response times during encoding showed a significant main effect of congruence, $F(1,60) = 10.038$, $\eta^2_G = 0.004$, $p = .002$. It indicates significantly faster response times to congruent words ($M = 908.66$, $SEM = 29.21$ ms) as compared to incongruent words ($M = 932.35$, $SEM = 33.18$ ms) (Fig. 2A). There was no significant main effect of age and no significant interaction between age and congruence, $p > .1$.

A summary with participants' raw responses (percentages and absolute numbers) at the test phase can be found in Table 1. A first two-way mixed-design ANOVA with the factors age (young, old) and congruence (congruent, incongruent) on the corrected hit rates from the test phase (high confidence responses) showed a significant main effect of congruence, $F(1,60) = 547.18$, $\eta^2_G = 0.536$, $p < .001$. As expected, this was driven by higher corrected high confidence hit rates for congruent ($M = 54.38$, $SEM = 2.65\%$) as compared to incongruent ($M = 28.41$, $SEM = 2.48\%$) words (Fig. 2B). There was no significant effect of age and no significant interaction between age and congruence, $p > .1$.

A second ANOVA on the absolute numbers of old words with factors age (young, old) and confidence (sure, unsure) revealed a main effect of age, $F(1,60) = 10.6$, $\eta^2_G = 0.034$, $p = .002$, and main effect of confidence, $F(1,60) = 140.97$, $\eta^2_G = 0.653$, $p\langle < .001$. However, interaction between age and confidence was not statistically significant, $p\rangle > .1$. As expected, the main effect of confidence was driven by more high-confident responses ($M = 198.62$, $SEM = 6.41$) as compared to low-confident responses ($M = 67.95$, $SEM = 6.04$); see Table 1.

3.2. fMRI results

3.2.1. Encoding phase

Clusters, peak coordinates and cytoarchitectonic probabilities for the main effect of congruence and main effect of age are shown in Supplementary Tables S1-S3. For the main effect of age, young vs. old revealed significantly higher activation within the entire MTL including the bilateral hippocampal subfields CA1 and CA3, bilateral laterobasal amygdala, dentate gyrus and entorhinal cortex (Supplementary Figure S1). However, there was no significantly higher activation for old vs. young. For the main effect of congruence, congruent vs. incongruent words also revealed increased activation within bilateral hippocampal subfields, bilateral laterobasal amygdala, dentate gyrus, and subiculum (Fig. 3); incongruent vs. congruent words did not show any effects with the MTL or amygdala. The interaction between age and congruence also did not show significant effects within the MTL or amygdala.

3.2.2. DM and functional connectivity results

Clusters, peak coordinates and cytoarchitectonic probabilities are shown in Table 2. With this analysis, we aimed to identify those voxels showing significant positive DM effects for congruent and incongruent items (i.e., overall main effect) and, at the same time, a significantly stronger DM effect for congruent vs. incongruent items. Such a pattern was revealed using an inclusive conjunction analysis of the 'overall main effect of DM' ($p < .05$, FWE-corrected) together with the significant difference between DM congruent vs. DM incongruent ($p < .001$, uncorrected). This conjunction analysis revealed a significant activation within the right hippocampus. Using the cytoarchitectonic toolbox, this cluster could be identified as being located within CA3 with a probability of 74% (Fig. 4A, B). As expected, the pattern of the beta values

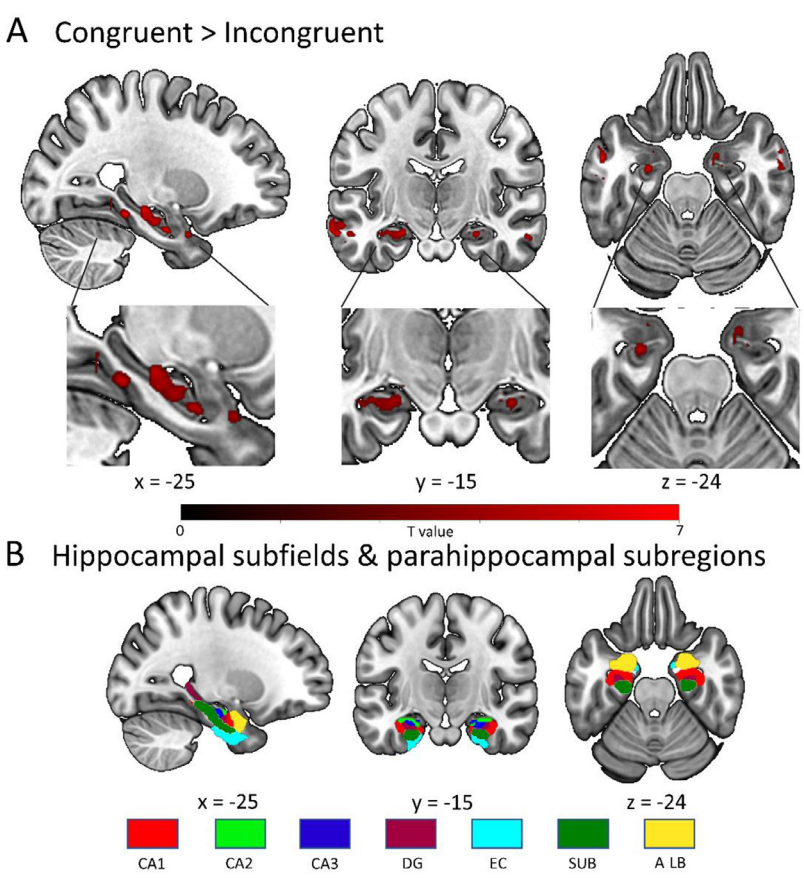

Fig. 3. (A) Main effect of congruence. Congruent vs. incongruent items were associated with significantly more activation within the MTL including the amygdala. The *t*-values are thresholded at $p < .05$ (FWE-corrected for multiple comparisons at the cluster level) and superimposed on a T1-weighted structural MNI template. (B) Depicts hippocampal subfields and parahippocampal subregions. Abbreviations: CA: cornu ammonis, DG: dentate gyrus, EC: entorhinal cortex, SUB: subiculum, A LB: laterobasal amygdala.

Table 2
DM and functional connectivity results for the two-factor mixed-design ANOVA. Clusters, peak coordinates, *F*-values and cytoarchitectonic probabilities are reported for MTL regions including hippocampus and adjacent amygdala. All results are FWE-corrected at the cluster level, $p < .05$. Abbreviation: *k*: cluster size, CA: cornu ammonis, LB: laterobasal.

Cluster	x	y	z	*k*	Cytoarchitectonic probability	Peak *F* value	p_{FWE}-value
DM results							
Overall main effect in conjunction with (DM Congruent sure > DM Incongruent sure)							
Cluster 1	22	−17	−18	14	–	–	0.034
Local maxima 1	22	−17	−18	–	–	24.10	–
R CA3	–	–	–	–	74%	–	–
R CA2	–	–	–	–	3%	–	–
Functional connectivity results							
Overall main effect in conjunction with (DM Congruent sure > DM Incongruent sure)							
Cluster 1	29	1	−23	60	–	–	< 0.001
Local maxima 1	30	−3	−23	–	–	123.63	–
R Amygdala (LB)	–	–	–	–	56%	–	–

for each condition imply that the DM effect is positive for congruent and incongruent items, and it is more pronounced for congruent items (Fig. 4C). Note that the CA3 activation for the DM effect (x, y, z: 22, −17, −18) was observed at a nearly identical position as local maxima 2 in cluster 2 of the congruence effect (x, y, z: 21, −20, −19, Table S3).

Other contrasts for the DM analysis (main effects of congruence, main effect of age, and interaction) did not reveal any significant effects. Specifically, there was no significant effect for the contrast DM incongruent vs. DM congruent even at a liberal threshold of $p < .005$ (uncorrected).

For the functional connectivity analysis, voxels demonstrating the effect within the right hippocampus (CA3, showing a more pronounced DM effect for congruent vs. incongruent items, Fig. 4A) were used as seed region. It revealed a significant effect within the right laterobasal amygdala (LB, Fig. 4D), indicating a significant functional coupling between both brain regions (Fig. 4C, D).

Since we were specifically interested in the network underlying the positive effect of congruence on subsequent memory, we only performed the functional connectivity analysis on the corresponding DM contrast but not the congruence effect per se (congruent vs. incongruent items).

4. Discussion

In this study, we used high resolution fMRI of the MTL in healthy humans to investigate the relationship between semantic congruence processing and the formation of subsequent long-term memory. Within the MTL, several hippocampal subfields, including the subiculum, CA1, CA3 and dentate gyrus, as well as the entorhinal cortex and laterobasal amygdala responded to semantic congruence suggesting that schema representation is supported by a widespread functional MTL network. Importantly, the positive effects of semantic congruence on subsequent memory could specifically be linked to CA3 and the functionally cou-

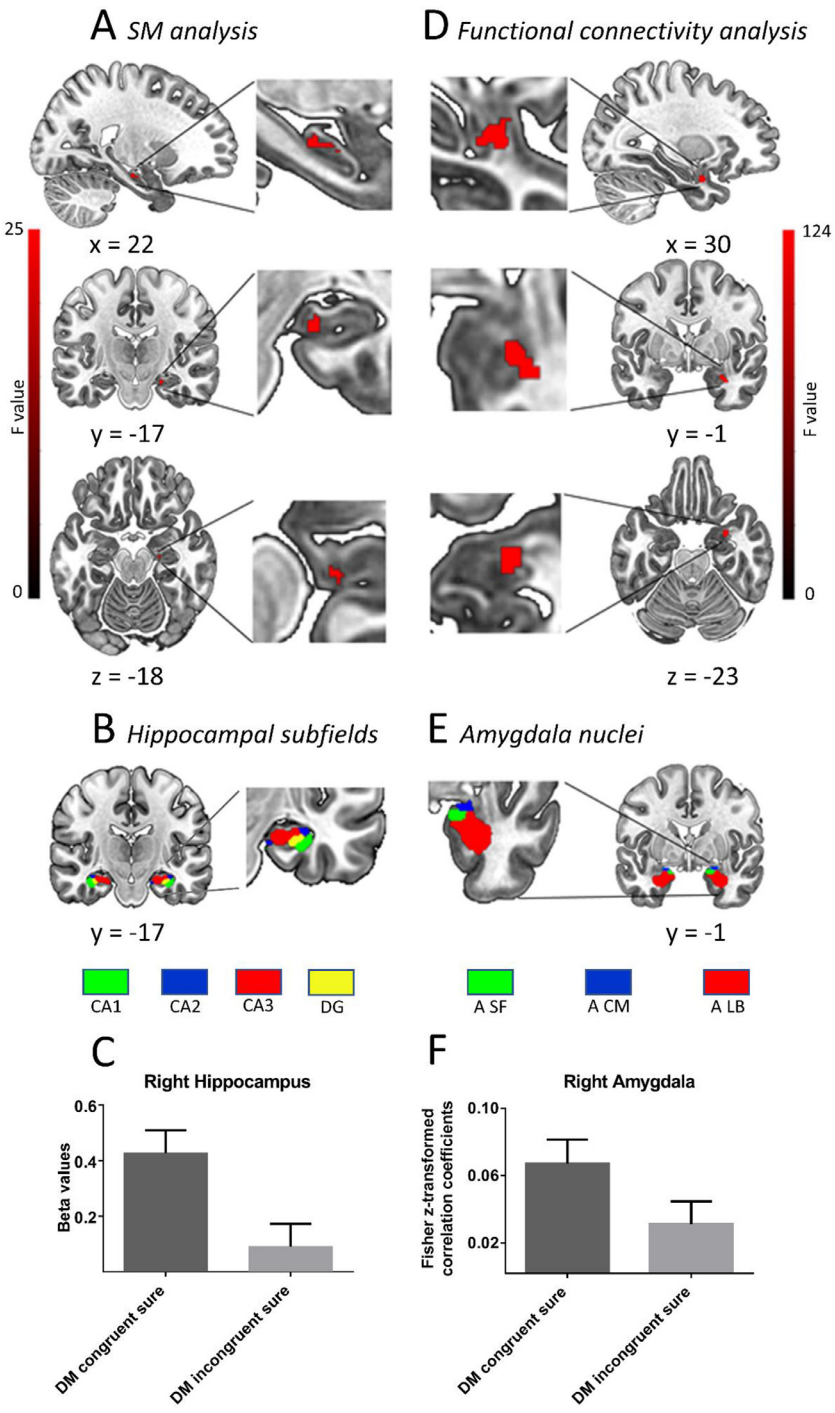

Fig. 4. Subsequent memory (SM) analysis and functional connectivity results. (A) A significantly stronger DM-effect for congruent vs. incongruent items was associated with activation in CA3. (D) This cluster showed functional connectivity with the laterobasal amygdala. For visualization purpose, (B) depicts hippocampal subfields and (E) amygdala nuclei based on the probabilistic atlas as derived from the SPM Anatomy toolbox. Bar graphs demonstrate the pattern of activation within (C) the right hippocampus and (F) right amygdala. The *F*-values are thresholded at $p < .05$ (FWE-corrected for multiple comparisons at the cluster level) and superimposed on a T1-weighted structural MNI template. Abbreviations: CA: cornu ammonis, DG: dentate gyrus, A SF: superficial amygdala, A CM: centromedial amygdala, A LB: laterobasal amygdala.

pled laterobasal amygdala. As such, our results indicate that, during encoding, schema-dependent processes drive memory integration within specific and interconnected MTL subregions.

In line with previous literature (Craik and Tulving, 1975; Packard et al., 2020, 2017; Schulman, 1974), congruent items were subsequently better recognized than incongruent items (Fig. 2). In cognitive psychology, this effect has often been explained on the basis of schema related processing, suggesting that semantic congruency drives the integration of information into preexisting knowledge structures (Piaget, 1952). In our case, the initial presentation of a semantic category is supposed to activate its semantic representation, and, in case of a congruent subsequent word, its integration is being promoted. Such a view is also compatible with faster response times for congruent words, further indicating accelerated information processing by semantic congruence. Importantly, the memory advantage by semantic congruence was evident in both healthy young and older participants. While age-related impairments could have been expected on the basis of well-described memory deficits in older adults, it is also clear that semantic memory (i.e., long-term memory for facts that are independent of time and date) is often preserved until old age (Hedden and Gabrieli, 2004; Ofen and Shing, 2013). Together with no significant interactions between congruence and age at the neural level (results), and evidence from two recent EEG studies (Crespo-Garcia et al., 2012; Packard et al., 2020), this provides further evidence that the effects of semantic congruence on long-term recognition memory are robust during healthy aging. However, in some studies, congruence effects appeared to be impaired

during healthy aging. Specifically, in an associative memory task, in which subjects had to learn the link between groceries and realistic or unrealistic prices, memory performance for realistic (i.e. meaningful) prices did not differ between age groups, but older adults remember unrealistic prices worse that younger adults (Amer et al., 2019, 2018). This age effect was associated with additional brain activation in older as compared to younger adults (Amer et al., 2019), which we did not observe in our study. Together, there is only a limited number of published studies on age-related changes in the effect of congruence on long-term memory, and further research is needed.

At the neural level, semantic congruency was associated with rather widespread activations within the MTL (Fig. 3B). This is in line with previous work suggesting that the MTL, in concert with the prefrontal cortex, provides the neural basis for schema processing (Gilboa and Marlatte, 2017; van Kesteren et al., 2012). Our findings give new insights by showing that within the MTL several hippocampal subfields, namely the subiculum, CA1, CA3, and DG, as well as the surrounding EC and amygdala respond to congruent vs. incongruent information. This further suggests that the activation of congruent semantic representations recruits specific MTL subfields or regions (Amaral, 1993; Lavenex and Amaral, 2000). At least for CA1 and CA3, this is compatible with previous research in rats suggesting that both subfields show firing patterns compatible with schema representations (McKenzie et al., 2014). Since both CA1 and CA3 are anatomically interconnected as part of the trisynaptic path including projections from EC to DG to CA3 to CA1 (see introduction), it appears reasonable to assume that all four regions are involved in the process of matching specific instances with pre-activated schema representations.

The observation of enhanced MTL activation for semantic congruence is particularly important since it helps to refine our theoretical understanding of schema related memory formation. Specifically, the SLIMM model (van Kesteren et al., 2012) suggests that semantic congruent information leads to resonance in the mPFC, which, as a consequence, inhibits MTL activity in order to drive semantic integration. Indeed, initial studies are compatible with SLIMM (Bein et al., 2014; Brod et al., 2016; Reggev et al., 2016; van Kesteren et al., 2014, M.T.R. 2013, 2012) while others, including more recent ones, suggest that both the mPFC and MTL together drive semantic integration (Gilboa and Marlatte, 2017; Linden et al., 2017; Liu et al., 2017; McKenzie et al., 2014, S. 2013; Preston and Eichenbaum, 2013; Staresina et al., 2009; van Kesteren et al., 2020). For instance, Reggev et al. (2016) reported a hippocampal DM effect for incongruent information, which is in line with Brod et al. (2016) who showed reduced hippocampal activity for more relevant knowledge. In contrast, Staresina et al. (2009) found that right hippocampal activation for congruent vs. incongruent items correlated with the congruency memory benefit across participants, which is consistent with our findings. Specifically, on the basis of high-resolution fMRI, our findings clearly show enhanced MTL activation for semantic congruence, which provides further evidence that the MTL plays an active role in semantic integration. However, given that we acquired only a partial volume of the brain, we cannot draw any conclusions regarding the functional interaction between PFC and MTL. Moreover, it remains unclear under which circumstances the MTL shows a more active role during congruence dependent memory formation. One possibility, that deserves further systematic investigation, is that the hippocampus is more actively involved when the paradigm includes a temporal gap, which requires the integration of information across spatiotemporal discontiguities to allow associative memory formation (Davachi and DuBrow, 2015; Eichenbaum, 2014; MacDonald et al., 2011; Schapiro et al., 2012; Staresina and Davachi, 2009).

Another main finding of our work is a specific link between the subsequent memory effect by semantic congruence and enhanced activation of CA3 (Fig. 4A), which was functionally coupled to the laterobasal amygdala (Fig. 4B). CA3 receives input from DG, which is supposed to provide the anatomical basis for pattern separation. This process drives efficient encoding, subsequent storage and finally the retrieval of information in CA3 (Jonas and Lisman, 2014; Senzai, 2019). Although our data only speak to encoding activity, the observed activation pattern is in line with such a view and the notion that CA3 acts as “single attractor” or “autoassociation network” (Grande et al., 2019; Rolls, 2013a, 2013b). Given that CA3 activity for subsequently recognized information was significantly enhanced in the congruent condition, this indicates a modulation of regional activity through semantic congruence. While the specific computations underlying congruence dependent learning cannot be addressed in our work, a recent study suggests that, in associative learning tasks, the hippocampus drives cortical assimilation of new information by resolving interference between novel and already stored knowledge (Bein et al., 2020). Together, CA3 appears to be a specific anatomical hub for the positive effect of semantic congruence on long-term recognition memory, and the underlying process may relate to pattern separation.

During successful encoding of congruent semantic information, CA3 was functionally coupled to the laterobasal amygdala. This provides novel insights into the role of the amygdala and is compatible with its anatomical connection to the parahippocampal, entorhinal, and hippocampal cortices (Pitkänen et al., 2000; Ruiz-Rizzo et al., 2020; Strange et al., 2014) as well as its role in subsequent memory formation for neutral items (Rutishauser et al., 2010). Specifically, during the encoding of images, including animals, cars and tools, local theta-frequency phase-locking (3–8 Hz) within the amygdala predicted successful memory formation in humans (Rutishauser et al., 2010). Moreover, the laterobasal amygdala plays a critical role in fear-related learning and emotional memory encoding as shown in humans and animals (Hakamata et al., 2020; Nonaka et al., 2014; Rosenberger et al., 2019). Our findings provide further evidence that the amygdala is involved in learning emotionally neutral information and they suggest that a functional interplay between CA3 and the laterobasal amygdala is particularly important for the encoding of congruent semantic information. Again, since we focused on the MTL, it remains to be investigated how the interaction between CA3 and amygdala relates to other brain regions including the PFC.

Both age groups did not differ in their overall memory performance, which is in line with the notion of preserved semantic memory until old age. However, at the neural level, robust age differences could be observed (Fig. S1). Specifically, independent of congruence, younger adults displayed higher activity within bilateral hippocampus, amygdala, and parahippocampal gyrus indicating age-related functional differences, possibly impairments, in the underlying brain regions (Daugherty et al., 2015; Raz et al., 2005). Reduced hemodynamic MTL activation for older subjects has been reported before but typically in association with reduced behavioral performance (Berron et al., 2018; Reagh et al., 2020; Ryan et al., 2012). One possibility for the absence of behavioral differences despite reduced MTL activity is that other brain regions may have compensated for reduced MTL functioning leading to equivalent behavior. Indeed, while region specific activity increased in older subjects when task demands are low, at higher task demands this may flip and result in decreased brain activation and behavior (Cabeza et al., 2018; Reuter-Lorenz and Cappell, 2008). Apart from this hypothesized upregulation, or in other words shift in demand-activity function, which is mainly based on observations within the PFC during working memory (Cappell et al., 2010), other forms of compensation, namely selection and reorganization (Cabeza et al., 2018), are also possible. Alternatively, fMRI might be more sensitive in detecting physiological age-related effects, which may not necessarily be apparent at the behavioral level. Indeed, abnormal EEG measures during early stages of Alzheimer’s disease can predict a severe decline in cognitive functions even when behavioral changes are not yet evident (Helkala et al., 1991). Future research should address this issue by using a paradigm that systematically varies task demands and functional brain imaging covering the PFC.

Age-related differences in hemodynamic activity could be driven by changes in neurovascular coupling (Chen, 2019). For instance, in a pre-

vious study with fMRI and neuronal optical measures, hemodynamic activity to visual stimulation in BA17 was reduced in older humans but they had similar neurovascular coupling functions as compared to a group of younger subjects; however, there was an age-related decrease in the coupling between oxy- and deoxy-hemoglobin, which was further modulated by physical fitness (Fabiani et al., 2014). Partly compatible with this observation, work by others indicates that healthy aging, as investigated here, is not necessarily associated with significant changes in BOLD-related neurovascular coupling (Grinband et al., 2017). Together, vascular and metabolic brain changes may bias BOLD activity as measured with fMRI; therefore, differences in age-related fMRI activity should be interpreted with caution (see Chen, 2019 for review).

Finally, hippocampal subfield analyses can be performed in different ways all offering pros and cons. Our approach is mainly based on a normalization of high resolution anatomical and functional images that were related to cytoarchitectonic probability maps (see methods). This way does not require any manual segmentation steps and is, therefore, very reliable. While manual segmentation of anatomical data without normalization might be more precise, it requires intensive training and a reproduction could be biased by human factors. Finally, automatic segmentation of hippocampal subfields is also possible and might lead to comparable results (Wenger et al., 2014). A formal comparison of all three methods is beyond the scope of this research article, and needs to be addressed in future work. This might also include higher spatial resolution than 1.5 mm^3, for instance based on ultra-high field MRI, which could improve segmentation results (Giuliano et al., 2017; Wisse et al., 2021). Along these lines, it is important to note that, in our work, a clear distinction between CA3 and neighboring DG is difficult especially since we spatially normalized and smoothed.

Taken together, semantic congruence promotes long-term memory in both young and older adults, with no significant differences between age groups suggesting a robust beneficial effect across the life-span. At the neural level, semantic congruence could be linked to widespread activity within the MTL indicating an involvement of several hippocampal subfields and surrounding EC. Finally, CA3 was specifically associated with congruence dependent subsequent memory, and showed enhanced functional connectivity to the laterobasal amygdala. As such, our results give new insights into the functional properties of MTL subregions and they extend current models by demonstrating an active role of CA3 in concert with the laterobasal amygdala in schema-dependent memory formation.

Declaration of Competing Interest

The authors declare no competing interests.

Acknowledgment

This work was supported by a grant from the Deutsche Forschungsgemeinschaft (DFG, BU 2670/7-1 and BU 2670/7-2) to Nico Bunzeck, and a Juan de la Cierva Formación grant (FJC2018-037782-I) from the Ministerio de Ciencia y Innovación to Pau A. Packard.

Data availability

All data and analysis code are available from the corresponding author upon request, including a formal project outline. The data are not publicly available due to privacy regulations by the local ethics committee.

Credit author statement

P.A.P., L.F. and N.B. designed the study. M.Y., P.A.P. and N.B. analyzed data. M.Y. and N.B. wrote the article, and all the authors participated in revising it. All authors approved the submitted version.

Supplementary materials

Supplementary material associated with this article can be found, in the online version, at doi:10.1016/j.neuroimage.2021.118563.

References

Amaral, D.G., 1993. Emerging principles of intrinsic hippocampal organization. Curr. Opin. Neurobiol. 3, 225–229. doi:10.1016/0959-4388(93)90214-J.
Amaro, E., Barker, G.J., 2006. Study design in fMRI: basic principles. Brain Cogn 60, 220–232. doi:10.1016/j.bandc.2005.11.009.
Amer, T., Giovanello, K.S., Grady, C.L., Hasher, L., 2018. Age differences in memory for meaningful and arbitrary associations: a memory retrieval account. Psychol. Aging 33, 74–81. doi:10.1037/pag0000220.
Amer, T., Giovanello, K.S., Nichol, D.R., Hasher, L., Grady, C.L., 2019. Neural correlates of enhanced memory for meaningful associations with age. Cereb. Cortex 29, 4568–4579. doi:10.1093/cercor/bhy334.
Amunts, K., Kedo, O., Kindler, M., Pieperhoff, P., Mohlberg, H., Shah, N.J., Habel, U., Schneider, F., Zilles, K., 2005. Cytoarchitectonic mapping of the human amygdala, hippocampal region and entorhinal cortex: intersubject variability and probability maps. Anat. Embryol. (Berl.) 210, 343–352. doi:10.1007/s00429-005-0025-5.
Andersen, P., Morris, R., Amaral, D., Bliss, T., O'Keefe, J., 2006. The Hippocampus Book. Oxford University Press.
Ashburner, J., 2007. A fast diffeomorphic image registration algorithm. Neuroimage 38, 95–113. doi:10.1016/j.neuroimage.2007.07.007.
Bartlett, F.C., 1932. Remembering: A Study in Experimental and Social Psychology. Cambridge University Press, Cambridge.
Bein, O., Reggev, N., Maril, A., 2020. Prior knowledge promotes hippocampal separation but cortical assimilation in the left inferior frontal gyrus. Nat. Commun. 11, 4590. doi:10.1038/s41467-020-18364-1.
Berron, D., Neumann, K., Maass, A., Schütze, H., Fliessbach, K., Kiven, V., Jessen, F., Sauvage, M., Kumaran, D., Düzel, E., 2018. Age-related functional changes in domain-specific medial temporal lobe pathways. Neurobiol. Aging 0. doi:10.1016/j.neurobiolaging.2017.12.030.
Bower, G.H., 1972. Mental imagery and associative learning. In: Cognition in Learning and Memory. Wiley, New York, pp. 51–88.
Brett, M., Anton, J.L., Valabrgue, R., Poline, .J.-B., 2002. Region of interest analysis using an SPM toolbox. In: Presented at the 8th International Conference on Functional Mapping of the Human Brain, June 2-6, 2002, 13, Sendai, Japan, pp. 210–217 Neuroimage.
Cabeza, R., Albert, M., Belleville, S., Craik, F.I.M., Duarte, A., Grady, C.L., Lindenberger, U., Nyberg, L., Park, D.C., Reuter-Lorenz, P.A., Rugg, M.D., Steffener, J., Rajah, M.N., 2018. Maintenance, reserve and compensation: the cognitive neuroscience of healthy ageing. Nat. Rev. Neurosci. 1. doi:10.1038/s41583-018-0068-2.
Callaert, D.V., Ribbens, A., Maes, F., Swinnen, S.P., Wenderoth, N., 2014. Assessing age-related gray matter decline with voxel-based morphometry depends significantly on segmentation and normalization procedures. Front. Aging Neurosci. 6. doi:10.3389/fnagi.2014.00124.
Cappell, K.A., Gmeindl, L., Reuter-Lorenz, P.A., 2010. Age differences in prefontal recruitment during verbal working memory maintenance depend on memory load. Cortex J. Devoted Study Nerv. Syst. Behav. 46, 462–473. doi:10.1016/j.cortex.2009.11.009.
Chen, J., Olsen, R.K., Preston, A.R., Glover, G.H., Wagner, A.D., 2011. Associative retrieval processes in the human medial temporal lobe: hippocampal retrieval success and CA1 mismatch detection. Learn. Mem. 18, 523–528. doi:10.1101/lm.2135211.
Chen, J.J., 2019. Functional MRI of brain physiology in aging and neurodegenerative diseases. NeuroImage, Physiol. Quantitat. MRI 187, 209–225. doi:10.1016/j.neuroimage.2018.05.050.
Chua, E.F., Schacter, D.L., Sperling, R.A., 2009. Neural basis for recognition confidence in younger and older adults. Psychol. Aging 24, 139.
Craik, F.I.M., Tulving, E., 1975. Depth of processing and the retention of words in episodic memory. J. Exp. Psychol. Gen. 104, 268–294. doi:10.1037/0096-3445.104.3.268.
Crespo-Garcia, M., Cantero, J.L., Atienza, M., 2012. Effects of semantic relatedness on age-related associative memory deficits: the role of theta oscillations. Neuroimage 61, 1235–1248. doi:10.1016/j.neuroimage.2012.03.034.
Daugherty, A.M., Haacke, E.M., Raz, N., 2015. Striatal iron content predicts its shrinkage and changes in verbal working memory after two years in healthy adults. J. Neurosci. 35, 6731–6743. doi:10.1523/JNEUROSCI.4717-14.2015.
Dodson, C.S., Bawa, S., Krueger, L.E., 2007. Aging, metamemory, and high-confidence errors: a misrecollection account. Psychol. Aging 22, 122–133. doi:10.1037/0882-7974.22.1.122.
Edelstein, W.A., Glover, G.H., Hardy, C.J., Redington, R.W., 1986. The intrinsic signal-to-noise ratio in NMR imaging. Magn. Reson. Med. 3, 604–618. doi:10.1002/mrm.1910030413.
Eickhoff, S.B., Heim, S., Zilles, K., Amunts, K., 2006. Testing anatomically specified hypotheses in functional imaging using cytoarchitectonic maps. Neuroimage 32, 570–582. doi:10.1016/j.neuroimage.2006.04.204.
Eickhoff, S.B., Paus, T., Caspers, S., Grosbras, M.-.H., Evans, A.C., Zilles, K., Amunts, K., 2007. Assignment of functional activations to probabilistic cytoarchitectonic areas revisited. Neuroimage 36, 511–521. doi:10.1016/j.neuroimage.2007.03.060.
Eickhoff, S.B., Stephan, K.E., Mohlberg, H., Grefkes, C., Fink, G.R., Amunts, K., Zilles, K., 2005. A new SPM toolbox for combining probabilistic cytoarchitectonic maps and functional imaging data. Neuroimage 25, 1325–1335. doi:10.1016/j.neuroimage.2004.12.034.
Fabiani, M., Gordon, B.A., Maclin, E.L., Pearson, M.A., Brumback-Peltz, C.R., Low, K.A., McAuley, E., Sutton, B.P., Kramer, A.F., Gratton, G., 2014. Neurovascular coupling

in normal aging: a combined optical, ERP and fMRI study. Neuroimage 85 (Pt 1), 592–607. doi:10.1016/j.neuroimage.2013.04.113.
Freitas, S., Simões, M.R., Alves, L., Santana, I., 2013. Montreal cognitive assessment: validation study for mild cognitive impairment and Alzheimer disease. Alzheimer Dis. Assoc. Disord. 27, 37–43. doi:10.1097/WAD.0b013e3182420bfe.
Gilboa, A., Marlatte, H., 2017. Neurobiology of schemas and schema-mediated memory. Trends Cogn. Sci. 21, 618–631. doi:10.1016/j.tics.2017.04.013.
Giuliano, A., Donatelli, G., Cosottini, M., Tosetti, M., Retico, A., Fantacci, M.E., 2017. Hippocampal subfields at ultra high field MRI: an overview of segmentation and measurement methods. Hippocampus 27, 481–494. doi:10.1002/hipo.22717.
Göttlich, M., Beyer, F., Krämer, U., 2015. BASCO: a toolbox for task-related functional connectivity. Front. Syst. Neurosci. 9. doi:10.3389/fnsys.2015.00126.
Grande, X., Berron, D., Horner, A.J., Bisby, J.A., Düzel, E., Burgess, N., 2019. Holistic recollection via pattern completion involves hippocampal subfield CA3. J. Neurosci. 39, 8100–8111. doi:10.1523/JNEUROSCI.0722-19.2019.
Greiner, B., 2015. Subject pool recruitment procedures: organizing experiments with ORSEE. J. Econ. Sci. Assoc. 1 (1), 114–125.
Grinband, J., Steffener, J., Razlighi, Q.R., Stern, Y., 2017. BOLD neurovascular coupling does not change significantly with normal aging. Hum. Brain Mapp. 38, 3538–3551. doi:10.1002/hbm.23608.
Hakamata, Y., Mizukami, S., Izawa, S., Moriguchi, Y., Hori, H., Kim, Y., Hanakawa, T., Inoue, Y., Tagaya, H., 2020. Basolateral amygdala connectivity with subgenual anterior cingulate cortex represents enhanced fear-related memory encoding in anxious humans. Biol. Psychiatry Cogn. Neurosci. Neuroimaging 5, 301–310. doi:10.1016/j.bpsc.2019.11.008.
Hasselmo, M.E., Wyble, B.P., 1997. Free recall and recognition in a network model of the hippocampus: simulating effects of scopolamine on human memory function. Behav. Brain Res. 89, 1–34. doi:10.1016/S0166-4328(97)00048-X.
Hedden, T., Gabrieli, J.D.E., 2004. Insights into the ageing mind: a view from cognitive neuroscience. Nat. Rev. Neurosci. 5, 87–96. doi:10.1038/nrn1323.
Helkala, E.L., Laulumaa, V., Soininen, H., Partanen, J., Riekkinen, P.J., 1991. Different patterns of cognitive decline related to normal or deteriorating EEG in a 3-year follow-up study of patients with Alzheimer's disease. Neurology 41, 528–532. doi:10.1212/wnl.41.4.528.
Jonas, P., Lisman, J., 2014. Structure, function, and plasticity of hippocampal dentate gyrus microcircuits. Front. Neural Circuits 8. doi:10.3389/fncir.2014.00107.
Kesteren, M.T.R.van, Fernández, G., Norris, D.G., Hermans, E.J., 2010. Persistent schema-dependent hippocampal-neocortical connectivity during memory encoding and postencoding rest in humans. Proc. Natl. Acad. Sci. 107, 7550–7555. doi:10.1073/pnas.0914892107.
Kim, H., Cabeza, R., 2007. Trusting our memories: dissociating the neural correlates of confidence in veridical versus illusory memories. J. Neurosci. 27, 12190–12197. doi:10.1523/JNEUROSCI.3408-07.2007.
Komorowski, R.W., Garcia, C.G., Wilson, A., Hattori, S., Howard, M.W., Eichenbaum, H., 2013. Ventral hippocampal neurons are shaped by experience to represent behaviorally relevant contexts. J. Neurosci. 33, 8079–8087. doi:10.1523/JNEUROSCI.5458-12.2013.
Komorowski, R.W., Manns, J.R., Eichenbaum, H., 2009. Robust conjunctive item–place coding by hippocampal neurons parallels learning what happens where. J. Neurosci. 29, 9918–9929. doi:10.1523/JNEUROSCI.1378-09.2009.
Lavenex, P., Amaral, D.G., 2000. Hippocampal-neocortical interaction: a hierarchy of associativity. Hippocampus 10, 420–430.
LeDoux, J.E., 2014. Coming to terms with fear. Proc. Natl. Acad. Sci. 111, 2871–2878. doi:10.1073/pnas.1400335111.
Lisman, J.E., Grace, A.A., 2005. The hippocampal-VTA loop: controlling the entry of information into long-term memory. Neuron 46, 703–713.
Liu, Z.-.X., Grady, C., Moscovitch, M., 2017. Effects of prior-knowledge on brain activation and connectivity during associative memory encoding. Cereb. Cortex 27, 1991–2009. doi:10.1093/cercor/bhw047.
McKenzie, S., Frank, A.J., Kinsky, N.R., Porter, B., Rivière, P.D., Eichenbaum, H., 2014. Hippocampal representation of related and opposing memories develop within distinct, hierarchically organized neural schemas. Neuron 83, 202–215. doi:10.1016/j.neuron.2014.05.019.
McKenzie, S., Robinson, N.T.M., Herrera, L., Churchill, J.C., Eichenbaum, H., 2013. Learning causes reorganization of neuronal firing patterns to represent related experiences within a hippocampal schema. J. Neurosci. 33, 10243–10256. doi:10.1523/JNEUROSCI.0879-13.2013.
Murphy, K., Bodurka, J., Bandettini, P.A., 2007. How long to scan? The relationship between fMRI temporal signal to noise and necessary scan duration. Neuroimage 34, 565–574. doi:10.1016/j.neuroimage.2006.09.032.
Nasreddine, Z.S., Phillips, N.A., Bédirian, V., Charbonneau, S., Whitehead, V., Collin, I., Cummings, J.L., Chertkow, H., 2005. The Montreal cognitive assessment, MoCA: a brief screening tool for mild cognitive impairment. J. Am. Geriatr. Soc. 53, 695–699. doi:10.1111/j.1532-5415.2005.53221.x.
Nonaka, A., Toyoda, T., Miura, Y., Hitora-Imamura, N., Naka, M., Eguchi, M., Yamaguchi, S., Ikegaya, Y., Matsuki, N., Nomura, H., 2014. Synaptic plasticity associated with a memory engram in the basolateral amygdala. J. Neurosci. 34, 9305–9309. doi:10.1523/JNEUROSCI.4233-13.2014.
Ofen, N., Shing, Y.L., 2013. From perception to memory: changes in memory systems across the lifespan. Neurosci. Biobehav. Rev. 37, 2258–2267. doi:10.1016/j.neubiorev.2013.04.006.
Packard, P.A., Rodríguez-Fornells, A., Bunzeck, N., Nicolás, B., Diego-Balaguer, R., de, Fuentemilla, L., 2017. Semantic congruence accelerates the onset of the neural signals of successful memory encoding. J. Neurosci. 37, 291–301. doi:10.1523/JNEUROSCI.1622-16.2017.
Packard, P.A., Steiger, T.K., Fuentemilla, L., Bunzeck, N., 2020. Neural oscillations and event-related potentials reveal how semantic congruence drives long-term memory in both young and older humans. Sci. Rep. 10, 9116. doi:10.1038/s41598-020-65872-7.
Paller, K.A., Kutas, M., Mayes, A.R., 1987. Neural correlates of encoding in an incidental learning paradigm. Electroencephalogr. Clin. Neurophysiol. 67, 360–371. doi:10.1016/0013-4694(87)90124-6.
Piaget, J., 1952. The Origins of Intelligence in Children. International universities press, inc., New York.
Pitkänen, A., Pikkarainen, M., Nurminen, N., Ylinen, A., 2000. Reciprocal connections between the amygdala and the hippocampal formation, perirhinal cortex, and postrhinal cortex in rat: a review. Ann. N. Y. Acad. Sci. 911, 369–391. doi:10.1111/j.1749-6632.2000.tb06738.x.
Preston, A.R., Eichenbaum, H., 2013. Interplay of hippocampus and prefrontal cortex in memory. Curr. Biol. 23, R764–R773. doi:10.1016/j.cub.2013.05.041.
Raz, N., Lindenberger, U., Rodrigue, K.M., Kennedy, K.M., Head, D., Williamson, A., Dahle, C., Gerstorf, D., Acker, J.D., 2005. Regional brain changes in aging healthy adults: general trends, individual differences and modifiers. Cereb. Cortex 15, 1676–1689. doi:10.1093/cercor/bhi044.
Raz, N., Rodrigue, K.M., Head, D., Kennedy, K.M., Acker, J.D., 2004. Differential aging of the medial temporal lobe A study of a five-year change. Neurology 62, 433–438. doi:10.1212/01.WNL.0000106466.09835.46.
Reagh, Z.M., Delarazan, A.I., Garber, A., Ranganath, C., 2020. Aging alters neural activity at event boundaries in the hippocampus and posterior medial network. Nat. Commun. 11, 3980. doi:10.1038/s41467-020-17713-4.
Reuter-Lorenz, P.A., Cappell, K.A., 2008. Neurocognitive aging and the compensation hypothesis. Curr. Dir. Psychol. Sci. 17, 177–182. doi:10.1111/j.1467-8721.2008.00570.x.
Rissman, J., Gazzaley, A., D'Esposito, M., 2004. Measuring functional connectivity during distinct stages of a cognitive task. Neuroimage 23, 752–763. doi:10.1016/j.neuroimage.2004.06.035.
Robin, J., Moscovitch, M., 2017. Details, gist and schema: hippocampal–neocortical interactions underlying recent and remote episodic and spatial memory. Curr. Opin. Behav. Sci., Mem Time Space 17, 114–123. doi:10.1016/j.cobeha.2017.07.016.
Roediger, H.L., McDermott, K.B., 1995. Creating false memories: remembering words not presented in lists. J. Exp. Psychol. Learn. Mem. Cogn. 21, 803–814. doi:10.1037/0278-7393.21.4.803.
Rolls, E.T., 2013a. A quantitative theory of the functions of the hippocampal CA3 network in memory. Front. Cell. Neurosci. 7, 98. doi:10.3389/fncel.2013.00098.
Rolls, E.T., 2013b. The mechanisms for pattern completion and pattern separation in the hippocampus. Front. Syst. Neurosci. 7. doi:10.3389/fnsys.2013.00074.
Rosenberger, L.A., Eisenegger, C., Naef, M., Terburg, D., Fourie, J., Stein, D.J., van Honk, J., 2019. The human basolateral amygdala is indispensable for social experiential learning. Curr. Biol. 29, 3532–3537. doi:10.1016/j.cub.2019.08.078, e3.
Ruiz-Rizzo, A.L., Beissner, F., Finke, K., Müller, H.J., Zimmer, C., Pasquini, L., Sorg, C., 2020. Human subsystems of medial temporal lobes extend locally to amygdala nuclei and globally to an allostatic-interoceptive system. Neuroimage 207, 116404. doi:10.1016/j.neuroimage.2019.116404.
Rutishauser, U., Mamelak, A.N., Schuman, E.M., 2006. Single-trial learning of novel stimuli by individual neurons of the human hippocampus-amygdala complex. Neuron 49, 805–813. doi:10.1016/j.neuron.2006.02.015.
Rutishauser, U., Ross, I.B., Mamelak, A.N., Schuman, E.M., 2010. Human memory strength is predicted by theta-frequency phase-locking of single neurons. Nature 464, 903–907. doi:10.1038/nature08860.
Ryan, L., Cardoza, J.A., Barense, M.D., Kawa, K.H., Walletin-Flores, J., Arnold, W.T., Alexander, G.E., 2012. Age-related impairment in a complex object discrimination task that engages perirhinal cortex. Hippocampus 22, 1978–1989. doi:10.1002/hipo.22069.
Schulman, A.I., 1974. Memory for words recently classified. Mem. Cognit. 2, 47–52. doi:10.3758/BF03197491.
Senzai, Y., 2019. Function of local circuits in the hippocampal dentate gyrus-CA3 system. Neurosci. Res., Circ. Neural Dyn. Underlying Behav. 140, 43–52. doi:10.1016/j.neures.2018.11.003.
Sheth, A., Berretta, S., Lange, N., Eichenbaum, H., 2008. The amygdala modulates neuronal activation in the hippocampus in response to spatial novelty. Hippocampus 18, 169–181. doi:10.1002/hipo.20380.
Shing, Y.L., Werkle-Bergner, M., Li, S.-.C., Lindenberger, U., 2009. Committing memory errors with high confidence: older adults do but children don't. Memory 17, 169–179. doi:10.1080/09658210802190596.
Sommer, T., 2017. The emergence of knowledge and how it supports the memory for novel related information. Cereb. Cortex 27, 1906–1921. doi:10.1093/cercor/bhw031.
Spalding, K.N., Jones, S.H., Duff, M.C., Tranel, D., Warren, D.E., 2015. Investigating the neural correlates of schemas: ventromedial prefrontal cortex is necessary for normal schematic influence on memory. J. Neurosci. 35, 15746–15751. doi:10.1523/JNEUROSCI.2767-15.2015.
Squire, L.R., Stark, C.E.L., Clark, R.E., 2004. The medial temporal lobe*. Annu. Rev. Neurosci. 27, 279–306. doi:10.1146/annurev.neuro.27.070203.144130.
Strange, B.A., Witter, M.P., Lein, E.S., Moser, E.I., 2014. Functional organization of the hippocampal longitudinal axis. Nat. Rev. Neurosci. 15, 655–669. doi:10.1038/nrn3785.
Tse, D., Langston, R.F., Kakeyama, M., Bethus, I., Spooner, P.A., Wood, E.R., Witter, M.P., Morris, R.G.M., 2007. Schemas and memory consolidation. Science 316, 76–82. doi:10.1126/science.1135935.
Tse, D., Takeuchi, T., Kakeyama, M., Kajii, Y., Okuno, H., Tohyama, C., Bito, H., Morris, R.G.M., 2011. Schema-dependent gene activation and memory encoding in neocortex. Science 333, 891–895. doi:10.1126/science.1205274.
van Kesteren, M.T.R., Beul, S.F., Takashima, A., Henson, R.N., Ruiter, D.J., Fernández, G., 2013. Differential roles for medial prefrontal and medial temporal cortices in schema-dependent encoding: from congruent to incongruent. Neu-

ropsychol., Special Issue Funct. Neuroimaging Episod. Mem. 51, 2352–2359. doi:10.1016/j.neuropsychologia.2013.05.027.

van Kesteren, M.T.R., Rignanese, P., Gianferrara, P.G., Krabbendam, L., Meeter, M., 2020. Congruency and reactivation aid memory integration through reinstatement of prior knowledge. Sci. Rep. 10, 4776. doi:10.1038/s41598-020-61737-1.

van Kesteren, M.T.R., Rijpkema, M., Ruiter, D.J., Morris, R.G.M., Fernández, G., 2014. Building on prior knowledge: schema-dependent encoding processes relate to academic performance. J. Cogn. Neurosci. 26, 2250–2261. doi:10.1162/jocn_a_00630.

van Kesteren, M.T.R., Ruiter, D.J., Fernández, G., Henson, R.N., 2012. How schema and novelty augment memory formation. Trends Neurosci 35, 211–219. doi:10.1016/j.tins.2012.02.001.

Wenger, E., Mårtensson, J., Noack, H., Bodammer, N.C., Kühn, S., Schaefer, S., Heinze, H.-J., Düzel, E., Bäckman, L., Lindenberger, U., Lövdén, M., 2014. Comparing manual and automatic segmentation of hippocampal volumes: reliability and validity issues in younger and older brains. Hum. Brain Mapp. 35, 4236–4248. doi:10.1002/hbm.22473.

Wisse, L.E.M., Chételat, G., Daugherty, A.M., Flores, R.de, Joie, R.la, Mueller, S.G., Stark, C.E.L., Wang, L., Yushkevich, P.A., Berron, D., Raz, N., Bakker, A., Olsen, R.K., Carr, V.A., 2021. Hippocampal subfield volumetry from structural isotropic 1mm3 MRI scans: a note of caution. Hum. Brain Mapp. 42, 539–550. doi:10.1002/hbm.25234.

Witter, M.P., Groenewegen, H.J., Lopes da Silva, F.H., Lohman, A.H.M., 1989. Functional organization of the extrinsic and intrinsic circuitry of the parahippocampal region. Prog. Neurobiol. 33, 161–253. doi:10.1016/0301-0082(89)90009-9.